Interaction of mineral dust with gas phase nitric acid and sulfur dioxide during the MINATROC II field campaign: First estimate of the uptake coefficient g HNO 3 from atmospheric data

B. Umann, F Arnold, C Schaal, M. Hanke, J. Uecker, H. Aufmhoff, Yves Balkanski, R. van Dingenen

Interaction of mineral dust with gas phase nitric acid and sulfur dioxide during the MINATROC II field campaign: First estimate of the uptake coefficient γ_{HNO_3} from atmospheric data

B. Umann,[1] F. Arnold,[1] C. Schaal,[1] M. Hanke,[1] J. Uecker,[1] H. Aufmhoff,[1] Y. Balkanski,[2] and R. Van Dingenen[3]

Received 22 February 2005; revised 6 May 2005; accepted 7 September 2005; published 29 November 2005.

[1] Mineral dust, one of the most abundant aerosols by mass in the atmosphere, may have a lasting but to date almost unexplored effect on the trace gases nitric acid (HNO_3) and sulfur dioxide (SO_2). These gases have an important influence on, for example, the tropospheric ozone cycle, aerosol formation or acid rain. Within the second part of the MINATROC project (Mineral Dust and Tropospheric Chemistry) we investigated the interaction of mineral dust with gaseous HNO_3 and SO_2. The measurements were performed on a high mountain plateau (Izaña, Tenerife, 2367 m asl) using the highly sensitive CIMS (Chemical Ionization Mass Spectrometry) technique. During five periods of medium and one period of high atmospheric dust load, the HNO_3 concentration decreased with increasing dust concentrations, and in all cases the HNO_3 detection limit was reached. From the HNO_3 decrease the uptake coefficient γ_{HNO_3} was calculated for the first time on the basis of in situ measurements. For the observed events, γ_{HNO_3} varied between 0.017 and 0.054. Moreover, during the dust events a significant decrease of ozone (O_3) of the order of 30% was detected. The measurements and the analyses made in this paper show that the direct uptake of O_3 on dust is a minor pathway for O_3 depletion compared to the indirect effect, i.e., HNO_3 depletion on dust which takes away a source of the O_3 precursors nitrogen oxides. In contrast, a general interaction between SO_2 and mineral dust was not observed. Positive as well as negative and no correlations between SO_2 and mineral dust were detected.

Citation: Umann, B., F. Arnold, C. Schaal, M. Hanke, J. Uecker, H. Aufmhoff, Y. Balkanski, and R. Van Dingenen (2005), Interaction of mineral dust with gas phase nitric acid and sulfur dioxide during the MINATROC II field campaign: First estimate of the uptake coefficient γ_{HNO_3} from atmospheric data, *J. Geophys. Res.*, *110*, D22306, doi:10.1029/2005JD005906.

1. Introduction

[2] The trace gases HNO_3 and SO_2 influence the atmospheric chemistry in manifold ways. For example, HNO_3 affects the tropospheric ozone cycle and thus the greenhouse effect through its production via NO_2 and OH or through the renoxification of the atmosphere (i.e., the recovery of NO_x; $NO_x = NO + NO_2$) via photolysis of HNO_3 or the reaction of HNO_3 with OH. SO_2 can be oxidized by the OH radical to form H_2SO_4. Because of its low vapor pressure, the latter may initiate aerosol formation via homogeneous nucleation (clustering of H_2O, H_2SO_4 and/or NH_3 molecules [*Korhonen et al.*, 1999]) or ion-induced nucleation (molecules cluster around an ion [*Arnold*, 1980; *Yu and Turco*, 2000; *Wilhelm et al.*, 2004]). Moreover, the growth of preexisting aerosols can be influenced by the uptake of SO_2 or HNO_3 via formation of sulfate or nitrate on the aerosol surface, leading among others to a changing number of cloud condensation nuclei or changing scatter and absorption properties of aerosols.

[3] Mineral dust represents one of the most abundant aerosols by mass in the atmosphere [*Andreae et al.*, 1986; *Penner et al.*, 2001]. Only recently mineral dust was recognized as a potential sink for HNO_3 [*Dentener et al.*, 1996; *Goodman et al.*, 2000; *Hanisch and Crowley*, 2001; *Liao et al.*, 2003] and SO_2 [*Ullerstam et al.*, 2002; *Usher et al.*, 2002]. To date, apart from the MINATROC project, the interaction between these gases and mineral dust has been investigated to our knowledge only in the laboratory, and different groups present uptake coefficients that differ considerably. The uptake coefficient or surface reaction probability γ is the fraction of collisions between gas phase substances and condensed phases that lead to irreversible uptake due to chemical reactions [*Finlayson-Pitts and Pitts*, 2000]. For HNO_3 and SO_2, respectively, values for γ measured in the laboratory vary between $\gamma_{HNO_3} = 2 \cdot 10^{-5}$ and 0.18 [*Fenter et al.*, 1995; *Goodman et al.*, 2000; *Underwood*

[1]Atmospheric Physics Division, Max-Planck-Institut für Kernphysik, Heidelberg, Germany.
[2]Laboratoire des Sciences du Climat et de l'Environnement, Centre National de la Recherche Scientifique/Commissariat à l'Energie Atomique, Gif-sur-Yvette, France.
[3]Institute for Environment and Sustainability, Joint Research Centre, European Commission, Ispra, Italy.

0148-0227/05/2005JD005906

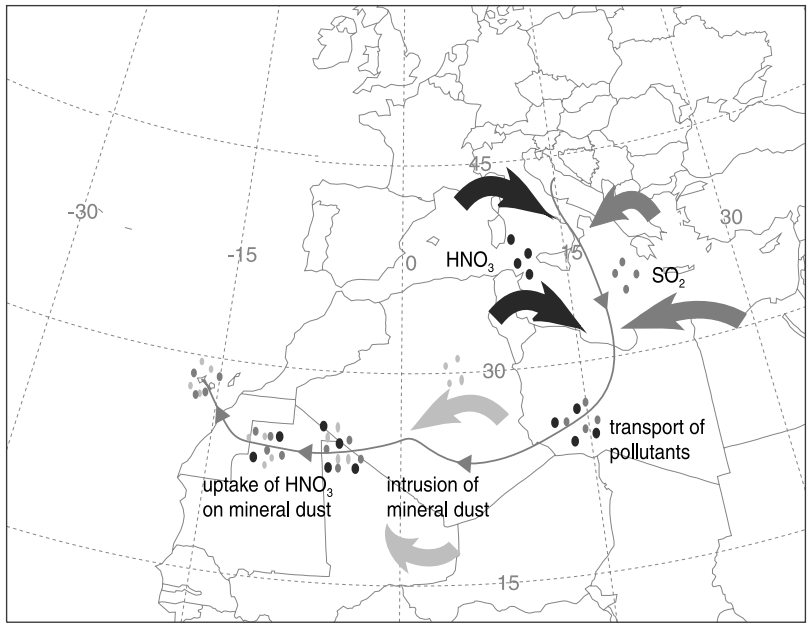

Figure 1. "Atmospheric flow reactor:" Pollutants such as HNO_3 (blue spots) or SO_2 (green spots) are injected into the atmosphere over south Europe or North Africa. Over northwest Africa these air masses mix with uplifted mineral dust (yellow spots), and heterogeneous reactions may take place. Here, only HNO_3 reacted with mineral dust. The picture is based on the backward trajectory from 29 July 2002, 1200 UTC, a day with high atmospheric dust load (NOAA, Washington, D. C., United States). See color version of this figure at back of this issue.

et al., 2001; *Hanisch and Crowley*, 2001] and $\gamma_{SO_2} = 10^{-7} - 5.1 \cdot 10^{-4}$ [*Ullerstam et al.*, 2002; *Usher et al.*, 2002], depending on the relative humidity (RH), the mass of the sample and the sample composition. Also, different groups use different surfaces (BET or geometric) to calculate the uptake coefficients. Calculated values for γ_{SO_2} lay between $3 \cdot 10^{-4}$ (assuming a deposition velocity of 0.03 m/s and for RH < 50%) and 0.1 (RH > 50% and high pH values) [*Dentener et al.*, 1996]. Which of these values are most realistic under atmospheric conditions is still an open question. To answer this question was part of our investigations.

[4] This work is embedded in the EU-funded project MINATROC which among others deals with the investigation of the interaction of mineral dust with gaseous HNO_3 and SO_2, aiming at a possible influence on tropospheric ozone. The measurements were performed using the highly sensitive CIMS technique. We found that HNO_3 reacts with mineral dust and that it was removed completely from the atmosphere at dust loads higher than $\sim$30 $\mu m^2/cm^3$. The HNO_3 decrease was accompanied by a decrease of O_3 of the order of 30%. In contrast, no significant correlation between SO_2 and mineral dust was observed.

[5] In the following we describe the project MINATROC and the CIMS apparatus used for the measurements of HNO_3 and SO_2, we present and discuss the collected data and suggest a value for the uptake coefficient γ_{HNO_3} on the basis of atmospheric measurements, we address to the observed O_3 decrease in the presence of dust and finally we summarize the results.

2. MINATROC Campaign

[6] MINATROC (Mineral Dust and Tropospheric Chemistry) was a European research project to examine the interaction of Saharan dust with various pollutants like HNO_3, SO_2 or O_3 in the atmosphere. MINATROC combines laboratory measurements, two field campaigns and atmospheric chemistry models. A brief overview of the project and a detailed general description of the first field campaign (MINATROC I) is given by *Balkanski et al.* [2003]. First results of MINATROC II regarding the measurements of RO_x, H_2O_2, NO_x, and O_3 can be found by *de Reus et al.* [2005]. Our group participated in both field campaigns with the measurement of, among others, gas phase nitric acid (HNO_3) and gas phase sulfur dioxide (SO_2). Our results of MINATROC I were presented by *Hanke et al.* [2003] and *Uecker et al.* [2001]. Here we discuss the results of the second field campaign (MINATROC II) at Izaña, Canary Islands, where only HNO_3 and SO_2 measurements were performed by our group.

2.1. Site Description

[7] Intensive field measurements were performed next to the GAW (global atmosphere watch) station Izaña Observatory, IZO, (28°18′N, 16°29′W) and 24 hour measurements were conducted from 15 July to 15 August 2002. The IZO is located on a plateau (2367 m asl) at Tenerife (Canary Islands, Spain). This site was chosen to examine the following scenario (Figure 1): Polluted air masses are lifted up by local convection (e.g., over Europe) and travel over the Sahara where they mix and react with uplifted dust. Consequently a dust concentration-dependent HNO_3 and SO_2 volume mixing ratio (VMR) was expected at Izaña. We point out that no Lagrangian experiments were performed. It cannot be excluded that no HNO_3-mineral dust interaction took place but that all air masses of interest were just free of pollutants like HNO_3, for example in the case of clean air masses from Africa. However, later on we discuss that this

was most likely not the case. Lagrangian experiments, e.g., with at least two measuring sites and/or aircrafts would be desirable but are, to my knowledge, not planned by now.

[8] Especially during daytime, local pollution from industrial areas or cities frequently reached the site (hereinafter called upslope events). Hence, for the calculation of γ_{HNO_3} we decided to consider only nighttime measurements (i.e., 2100–0600 UTC). During nighttime, pollution from local emissions is lower and, further on, in the majority of cases the site was in the free troposphere. However, obvious upslope events during nighttime (identifiable from the wind direction and from high concentrations of tracers for polluted air masses such as CO or SO_2) were removed from the data set.

[9] For the measurement of the rather "sticky" compound nitric acid it is important to keep distance from all surfaces where it can be adsorbed. Therefore we decided to set up the instrument in a measuring container slightly apart from the containers of the other groups and from the main buildings of IZO. The main wind directions were SE (during dust intrusions from the Sahara) and NW (air masses without dust). From Figure 2 it can be seen that our inlet was freely exposed to these wind directions.

2.2. Instrumentation

[10] The measurement of gaseous HNO_3 and SO_2 was performed using the CIMS technique (Chemical Ionization Mass Spectrometry) which was introduced for the measurement of atmospheric trace gases by our group [*Knop and Arnold*, 1985]. The CIMS probe was developed and built at the Max-Planck-Institut für Kernphysik in Heidelberg (MPI-K), Germany. Except for the inlet system (see below), the principle and the setup used for MINATROC II are the same as for MINATROC I and described in detail by *Hanke et al.* [2003], e.g., the CIMS probe or the production of the product ions CO_3^-. Here we only give a short overview.

[11] A sketch of the setup used at MINATROC II is shown in Figure 3. Atmospheric air enters a flow reactor (FR) via a high-volume blower inlet (HVBI) and a calibration line. Inside the FR the trace gases (HNO_3 and SO_2) react with ions (CO_3^-), which are selectively produced by an ion source (ion-molecule reaction, IMR). Finally, the formed cluster ions are detected by a quadrupole mass spectrometer (QMS). For details concerning the geometry, the ion source, the IMR inside the FR and the QMS we refer to *Hanke et al.* [2003]. For the sake of completeness we mention two slight changes compared to MINATROC I: First we lowered the temperature inside the calibration line and the FR from formerly 40°C to 30°C in order to lower the probability of evaporating HNO_3 from the aerosol phase. Second, to get rid of perturbing product ions in the mass spectra, we omitted completely the CO_2 supply for the ion source. In this case, the CO_3^- ions are produced by the ion source via natural CO_2 inside the FR and via CO_2 coming from impurities in the oxygen gas cylinder.

[12] All aerosol data used in this work were measured and calculated by the Institute for Environment and Sustainability, Joint Research Centre, JRC, Ispra, Italy. Fine particle size distributions (6–600 nm) were measured by means of a custom-built medium size Vienna type differential mobility analyzer (DMA), coarse particle size distributions (300 nm–10 μm) by means of an optical particle counter (OPC, Grimm dust monitor model 1.108) and the total aerosol mass (<10 μm) by means of a TEOM (tapered element oscillating microbalance).

2.2.1. Inlet System

[13] A potential problem concerning the measurement of gas phase HNO_3 via CIMS is the evaporation of HNO_3 from the aerosol phase inside the heated (30°C) and evacuated (50 hPa) calibration line and FR [see *Hanke et al.*, 2003]. The easiest way to avoid such HNO_3 contributions is to hinder aerosols from entering the instrument. Consequently we exchanged the sample line used at MINATROC I by the high-volume blower inlet (HVBI, left part of Figure 3). The HVBI consists of a stainless steel tube (2000 mm × 300 mm, i.d.) connected to two ventilators in series. The HVBI protrudes more than 1 m above the roof of the container so that the overall height above ground of the inlet is about 4 m. Perpendicular to the flux and in the center of this tube air is sucked into the instrument via a critical inlet orifice (i.d. ≈ 1.5 mm). "Critical orifice" means that the flux through the orifice depends only on its diameter and the pressure in front of the orifice. This guarantees a steady flux. The HVBI creates an air flux of ca. 1.2 m^3/s at almost 20 m/s. Because of this high flow velocity aerosols cannot follow the streamlines into the inlet orifice. To prove this we positioned an aerosol source (TSI-3076, constant output atomizer) in front of the critical orifice and adjusted different velocities inside the HVBI. At maximum speed no aerosols entered the instrument. The aerosol density for this experiment was in the region of $5 \cdot 10^5/cm^3$, according to the instruction manual of the aerosol source.

[14] The use of the HVBI implies another advantage: The formerly used, about 4000 mm long sampling line could be replaced by a calibration line of only 830 mm length. Therefore HNO_3 wall losses and the time necessary to reach equilibrium of HNO_3 mixing ratios could be reduced.

2.2.2. Diagnostic Measurements

[15] Reliable measurements imply a precise characterization of the instrument. Diagnostic measurements regarding wall losses on the HVBI, the inlet orifice and the calibration line were performed as well as regular calibrations and measurements of the background of the instrument. Laboratory studies have shown that SO_2 is not sensitive toward wall losses. Hence the results of these diagnostic measurements are addressed to HNO_3 and briefly presented in the following.

2.2.2.1. High-Volume Blower Inlet (HVBI)

[16] Because of its huge dimensions it was not possible to calibrate the HVBI. However, we can exclude losses of HNO_3 at the walls of the HVBI. Measurements with a calibrated alternative inlet system, consisting of a 4000 mm long Teflon tube, gave the same atmospheric HNO_3 VMR as with the HVBI, indicating that no significant amounts of HNO_3 adsorbs at the surfaces of the HVBI.

2.2.2.2. Inlet Orifice

[17] A critical point concerning HNO_3 wall losses is the (Teflon-) inlet orifice which is not calibrated in the conventional calibration mode (described below). Therefore we set up an additional calibration method with respect to the inlet orifice: HNO_3 calibration gas was introduced into the calibration line via a holed Teflon cylinder which was put over the inlet orifice. Compared to the conventional calibration mode the HNO_3 signal was about 15% lower.

Figure 2. Panorama of the measuring site Izaña. The picture was taken from the roof of our measuring container. See color version of this figure at back of this issue.

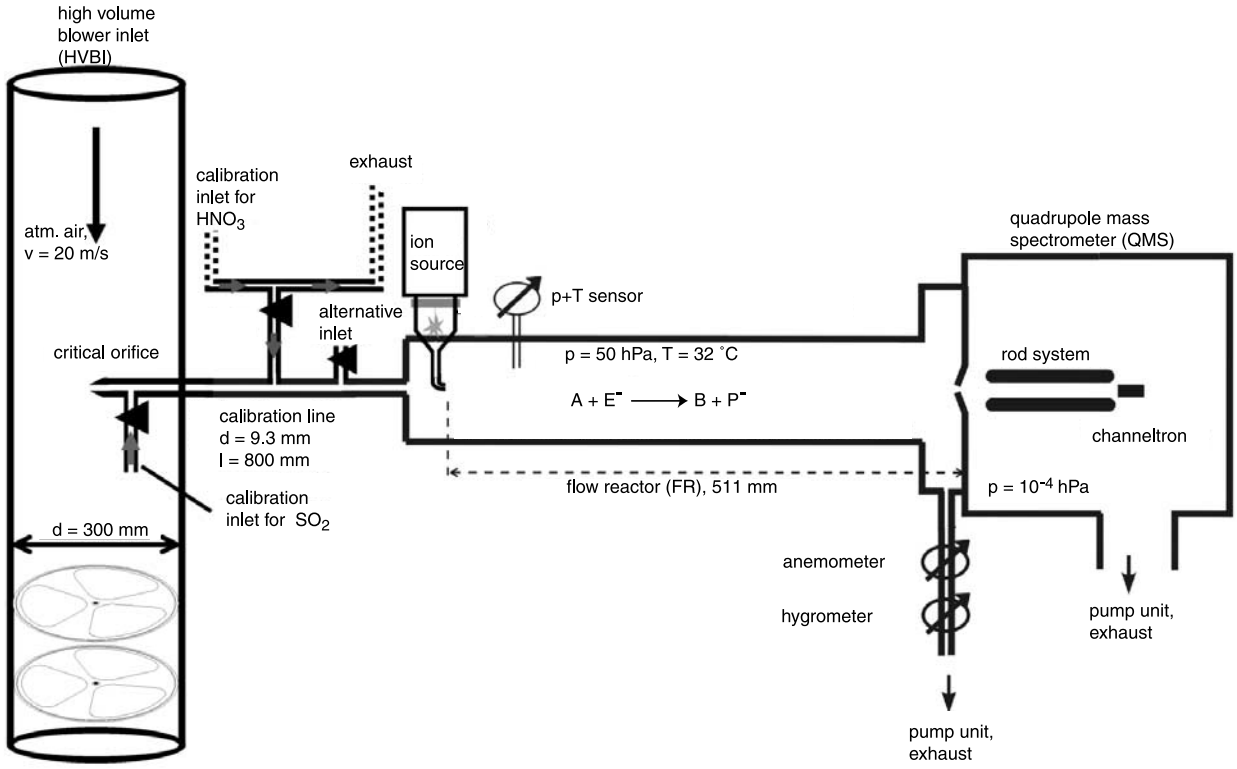

Figure 3. Sketch of the setup used at MINATROC II (not true to scale).

This can be considered as an upper limit for HNO_3 losses at the inlet orifice. However, these HNO_3 losses are most likely considerably lower since HNO_3 calibration gas gets lost at the Teflon cylinder itself. This is likely for two reasons: First because of the high pressure inside the cylinder (atmospheric pressure compared to 50 hPa inside the calibration line) and second for the rough surface of the noncommercial Teflon cylinder. Hence losses at the inlet orifice can be considered nonsignificant.

2.2.2.3. Calibration Line

[18] The calibration line is the part between the inlet orifice and the FR (see Figure 3) and consists of a Teflon tube (830 mm × 9.3 mm i.d.). Additional inlets for calibration gases and the alternative inlet are mounted here. This part of the setup is calibrated in any case and therefore not a critical point. However, the influence of Teflon material on gas phase HNO_3 is of scientific interest and was analyzed anyway. An investigation with and without calibration line showed no difference regarding the height of the HNO_3 mixing ratio, in agreement with *Neumann et al.* [1999]. The latter did not observe HNO_3 losses on various types of Teflon material as well. Nevertheless, in our study, equilibrium conditions were reached several minutes later when the calibration line was installed.

2.2.2.4. Background and Detection Limit

[19] Intensive background measurements and calibrations of the CIMS probe were performed at the site in the two weeks before and after the measurement period and almost daily within this period. The background measurement technique differs from that applied for MINATROC I [*Hanke et al.*, 2003] and will be described more detailed in the following.

[20] Note that this background measurement technique provides an upper limit for the detection limit: Measurements that were characterized by very low HNO_3 VMR (e.g., during a dust event and sometimes when the free troposphere reached the site) showed a high precision. This means that CIMS is able to measure low HNO_3 concentrations with a high rate of reproducibility. The method to measure the background described below does not provide as low HNO_3 VMR with such a high precision as nature does. Therefore, only for the dust events we decided to apply the ''natural'' detection limit. The natural detection limits were obtained by calculating the standard deviation of the HNO_3 VMR during the periods of highest dust load for every single dust event. These periods lasted for every dust event at least 7 hours. The standard deviations for the six dust events varied only between 17 and 23 pptv. The aim of this work was to estimate the order of magnitude for γ_{HNO_3}. Therefore we decided to define the detection limit for the dust events as 1σ.

[21] The following method is valid for the nondust periods. Zero air (ZA, i.e., air free of pollutants) was produced by a commercial ZA generator (Breitfuß Messtechnik GmbH, Germany) and introduced into the calibration line using the holed Teflon cylinder described above

Table 1. HNO_3 and SO_2 Detection Limits[a]

Date	Detection Limit HNO_3, pptv	Detection Limit SO_2, pptv
15 July, 0000 UTC, to 27 July, 0000 UTC	78	18
28 July, 0000 UTC, to 31 July, 1600 UTC	34	15
31 July, 1600 UTC, to 4 August, 1930 UTC	87	48
4 August, 1930 UTC, to 16 August, 0000 UTC	50	15
E1	22	
E2	23	
E3	17	
E4	20	
E5	22	
E6	17	

[a]For SO_2, the given dates imply the detection limits for the dust events. For the dust events the detection limit for HNO_3 was defined as 1σ, otherwise 2σ (see text).

(see Inlet orifice). To approach atmospheric conditions, the initially dry ZA was moistened with distilled water, according to the actual prevailing ambient relative humidity. It was found that both for HNO_3 and SO_2 the background showed a significant dependence on the RH as long as the O_2 supply for the ion source was lower than 0.80 slpm. Generally the O_2 flux for the ion source is kept constant at 1.34 slpm, i.e., higher than 0.80 slpm. However, because of problems in the beginning of the campaign we had to lower the O_2 flux and adjust different values for O_2. Only in this case the background raised linearly with increasing RH. Otherwise, i.e., O_2 higher than 0.80 slpm, the background was constant and, in particular, did not depend on the relative humidity. An explanation for this behavior cannot be given by now. Probably we deal with a systematic error at low O_2 fluxes. However, intensive background measurements with all applied O_2 fluxes and at different RH were performed. For all applied O_2 fluxes we plotted the background versus the RH. In case the background depended on the RH ($O_2 <$ 0.80 slpm) a straight line was fitted to the plot and the standard error of estimate (hereinafter referred as SEE) was calculated. The detection limit was then defined as twice the SEE. For backgrounds which were not dependent on RH, and thus were constant, the detection limit was defined as twice the standard deviation. For HNO_3 the detection limit varied between 7 and 87 pptv and for SO_2 between 8 and 48 pptv. The appropriate detection limits are listed in Table 1. To avoid any possibility of confusion we mention again that the detection limit does not depend on the RH but only on the adjusted O_2 supply for the ion source.

2.2.2.5. Calibration of CIMS

[22] The general calibration technique of CIMS for the measurement of HNO_3 and SO_2 is motivated and described thoroughly by *Hanke et al.* [2003]. Typical time plots of calibration cycles can be found there as well. Hence here we only give a short description of the principle. A standard HNO_3 calibration gas is produced by means of a permeation source. The HNO_3 concentration of this standard is determined by ion chromatography. SO_2 calibrations were performed using a commercial gas mixture of 1.04 ppmv SO_2 in N_2. After switching to the background mode described above, these standard gases were introduced into the calibration line via a critical orifice (HNO_3) and a tube of 4 mm i.d. (SO_2), respectively, directly after the inlet orifice (see Figure 3). Typical calibration gas concentrations for HNO_3 were 200–4000 pptv and for SO_2 200–2000 pptv. Tests regarding the linearity of the instrument were performed for both HNO_3 and SO_2 and linearity was given. Exemplarily, a calibration with linearity test for HNO_3 is shown in Figure 4. From the respond of the instrument a calibration factor cf is calculated and applied to the atmospheric measurements. As for the background, only for low O_2 fluxes the cf for both SO_2 and HNO_3 depended on the RH. In Figure 5 the water dependence of cf for HNO_3 is shown for O_2 = 0.49 slpm. Note that the relative humidity inside the flow reactor FR is very low as a consequence of the low pressure inside the FR (50 hPa). The error of the instrument (accuracy) concerning the SO_2 measurement is of the order of 20%. For HNO_3 the accuracy depends on the adjusted O_2 fluxes. From 15 July

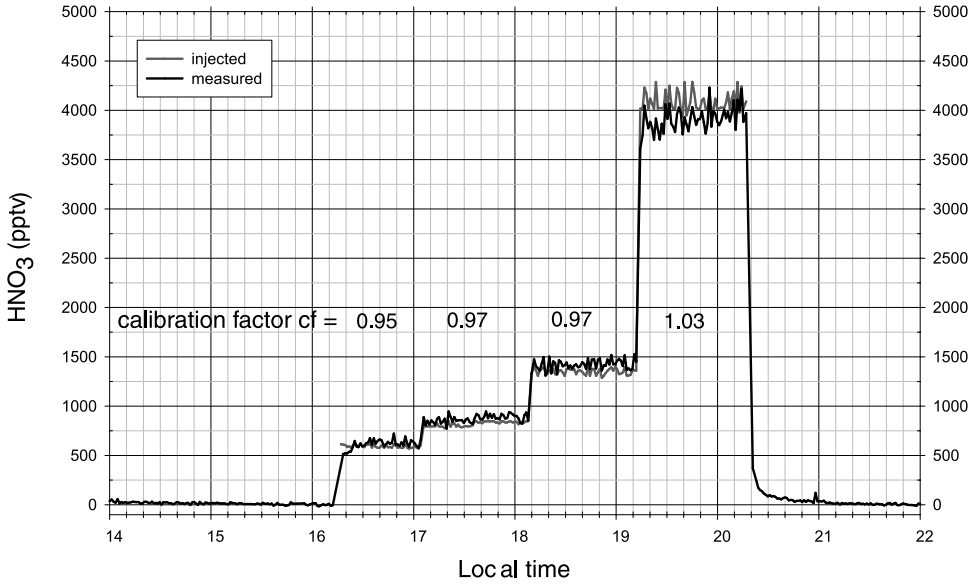

Figure 4. Test for the linearity of the HNO_3 calibration factor cf = $HNO_{3,injected}/HNO_{3,measured}$. Linearity is given. See color version of this figure at back of this issue.

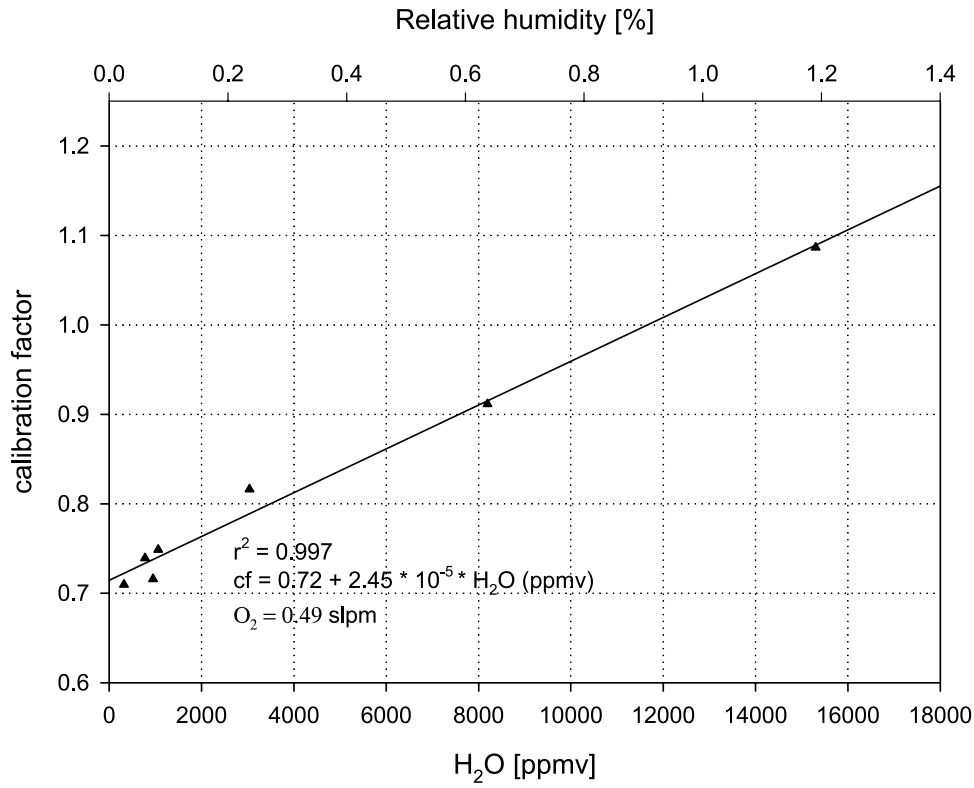

Figure 5. HNO_3 calibration factor cf as a function of the humidity inside the flow reactor. For further details, see text.

to 27 July it was ~35% and from 28 July to 15 August ~20%.

2.3. Observations

[23] During MINATROC II 6 periods of medium and high atmospheric dust load (hereafter called dust events or events) were observed at the site. According to backward trajectory calculations of the NOAA (national oceanic and atmospheric administration, Washington D.C., US) all these air masses originated from the Sahara or the Sahel, Northwest Africa. Each of the events lasted between 2 and 4 days. Five events were of almost the same intensity whereas the volume density during event number 3 (E3) exceeded the others fivefold to sevenfold. Table 2 gives an overview of the relevant dust data. Exemplarily, the average particle size distribution by volume PSDv and by number PSDn for E3, E4 and E5 is shown in Figure 6.

2.3.1. HNO_3

[24] Figure 7 shows the time series of the 30-min average values of the HNO_3 (and SO_2, RH) mixing ratios for the whole measurement period and Figure 8 shows the time series just for the dust events, together with the HNO_3 VMR as a function of the geometric dust surface area density (in the following referred just as surface area or only surface). Data from obvious upslope events are removed. Since upslope events could not always be identified unambiguously, the correlation plots are separated in daytime and nighttime measurements (daytime measurements are supposed to experience more frequently upslope events, see section 2.1). We defined day as 0600–2100 UTC and night as 2100–0600 UTC.

[25] For the six dust events the atmospheric HNO_3 VMR is highly significantly anticorrelated with dust and decreases with increasing dust concentrations (Figure 8). For surface areas higher than ~30 $\mu m^2/cm^3$ the detection limit is reached. Night and day mean values of HNO_3 drop from 307 and 302 pptv in dust-free air masses down to 47 and 114 pptv, respectively, during the dust events. Moreover, with high dust loads especially nighttime HNO_3 is significantly low (100 pptv are rarely exceeded) and its VMR

Table 2. Aerosol Data (Mean Values) for the Six Observed Dust Events (E1–E6)

	Date	Geometric Surface Density, $\mu m^2/cm^3$	Fuchs Surface Density, $\mu m^2/cm^3$	Volume Density, $\mu m^3/cm^3$	Collisional Lifetime t_c, s
E1	22–23 July	20.7	2.5	7.0	5298
E2	25–26 July	28.8	3.4	10.5	3896
E3	28–31 July	142.7	17.2	51.8	770
E4	5–7 August	35.5	4.3	12.6	3080
E5	9–10 August	20.8	2.4	7.9	5519
E6	12–13 August	25.7	3.1	9.5	4273
Without dust	rest	3.3	0.4	0.7	33113

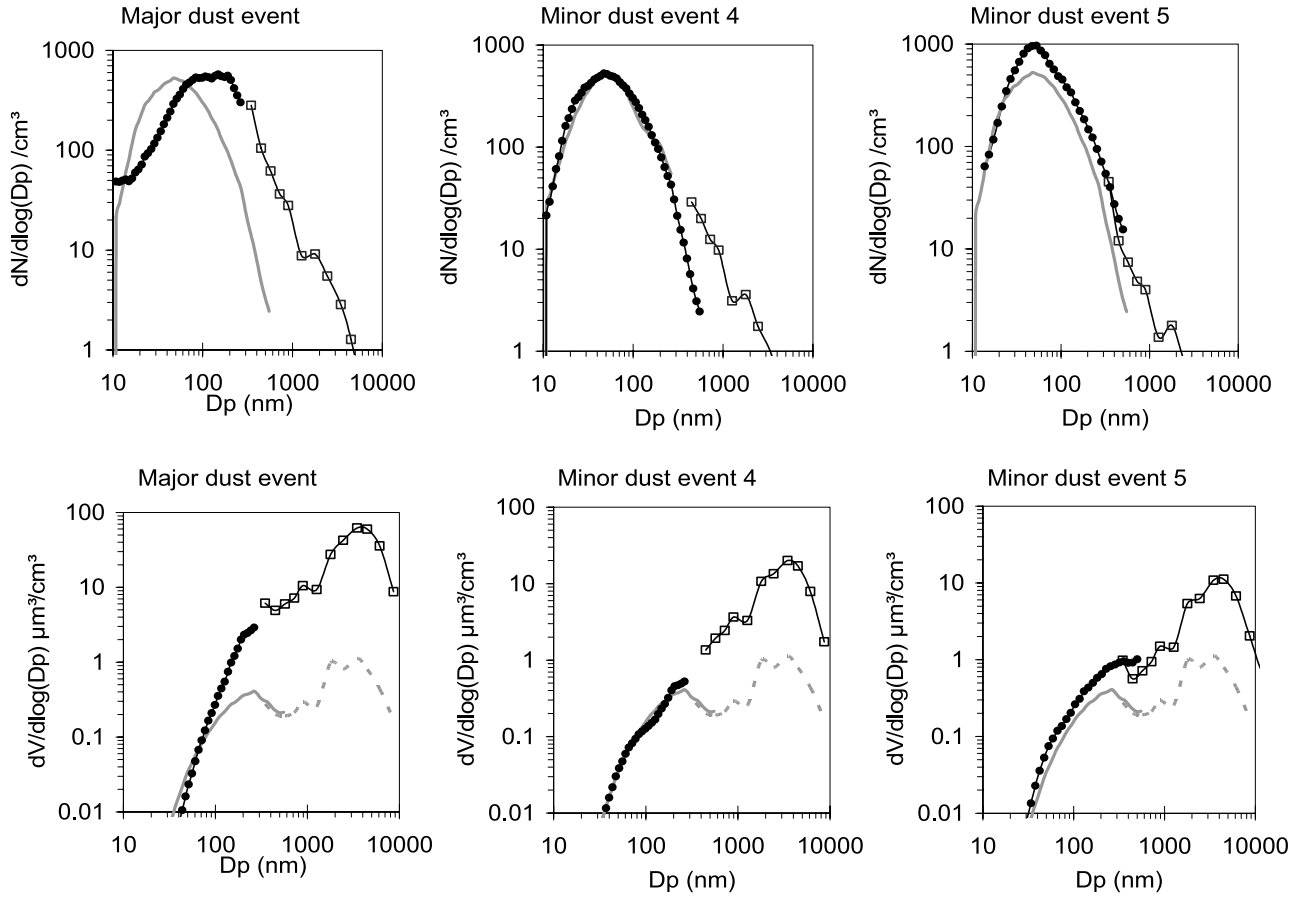

Figure 6. Average particle size distributions by number PSDn and by volume PSDv, exemplarily for the major dust event E3 and for the minor events E4 and E5. The lines with symbols represent the dust PSD. The line without symbols represents the PSD outside dust for comparison. The open squares and the shaded dashed line without symbols were measured by the OPC. The solid circles and the continuous shaded line without symbols were measured by the DMA.

never reaches the nondust mean value of 307 pptv. This is valid for all observed dust events.

[26] We can exclude that air masses originating from Africa are HNO_3-free per se. Our measurements together with backward trajectories show that African but dust-free air masses contained mean HNO_3 mixing ratios of the order of 300 pptv. This is in the same range as the mean value for all dust-free days. A summary of HNO_3 mean VMR categorized by the different air masses is shown in Table 3. Confirmation of HNO_3-containing air masses from the African west coast can be found by *Liao et al.* [2003] who present measurements of HNO_3 VMR from 250 to 450 pptv between ground level and 4200 m altitude. Almost all air masses which reached Izaña originated from the same level of altitude.

[27] During the dust events and in particular during night tracers for polluted air masses (such as CO, which is not supposed to react with mineral dust) showed no atypical behavior compared to the dust-free periods. This indicates that dust-rich air masses were ''normally polluted.'' On the other hand, HNO_3 as well is a tracer for polluted air masses since it is produced via NO_x. The main source of NO_x is the combustion of fossil fuels. Therefore, if no HNO_3-mineral dust interaction took place, the ratio of HNO_3 to CO in dust-rich air masses would be expected to stay in the same range as in dust-free air masses. Figure 9 shows that this is not the case. Depicted are the percentiles of the ratio of HNO_3 to CO versus the dust surface area, binned by 5 $\mu m^2/cm^3$ per bin. CO mixing ratios were measured by the Izaña Observatory (IZO) of the Spanish National Meteorological Institute (INM) and kindly put at our disposal. With no or low dust concentrations (0–5 $\mu m^2/cm^3$) this ratio is tenfold higher compared to periods with heavy dust loads (>30 $\mu m^2/cm^3$). This indicates that HNO_3 was removed from the atmosphere by mineral dust.

[28] Finally, we point out that an HNO_3 depletion due to sea salt aerosol over the Atlantic Ocean is possible [*Guimbaud et al.*, 2002] but not likely for MINATROC II. In Table 4 we present the minimal and maximal heights for each dust event, according to the backward trajectories of NOAA. We considered air masses from the moment of the dust intrusion until they reached Izaña and averaged over one day. According to *Seinfeld and Pandis* [1998], the sea salt concentration typically shows an exponential decrease with height. Thus, for the presented heights the sea salt concentration is in the range of 1.5–9% from the sea surface concentration. This is confirmed by the sea salt measurements of a participating group which are not ready for publication (J. P. Putaud, JRC, Ispra, personal communication, 2004).

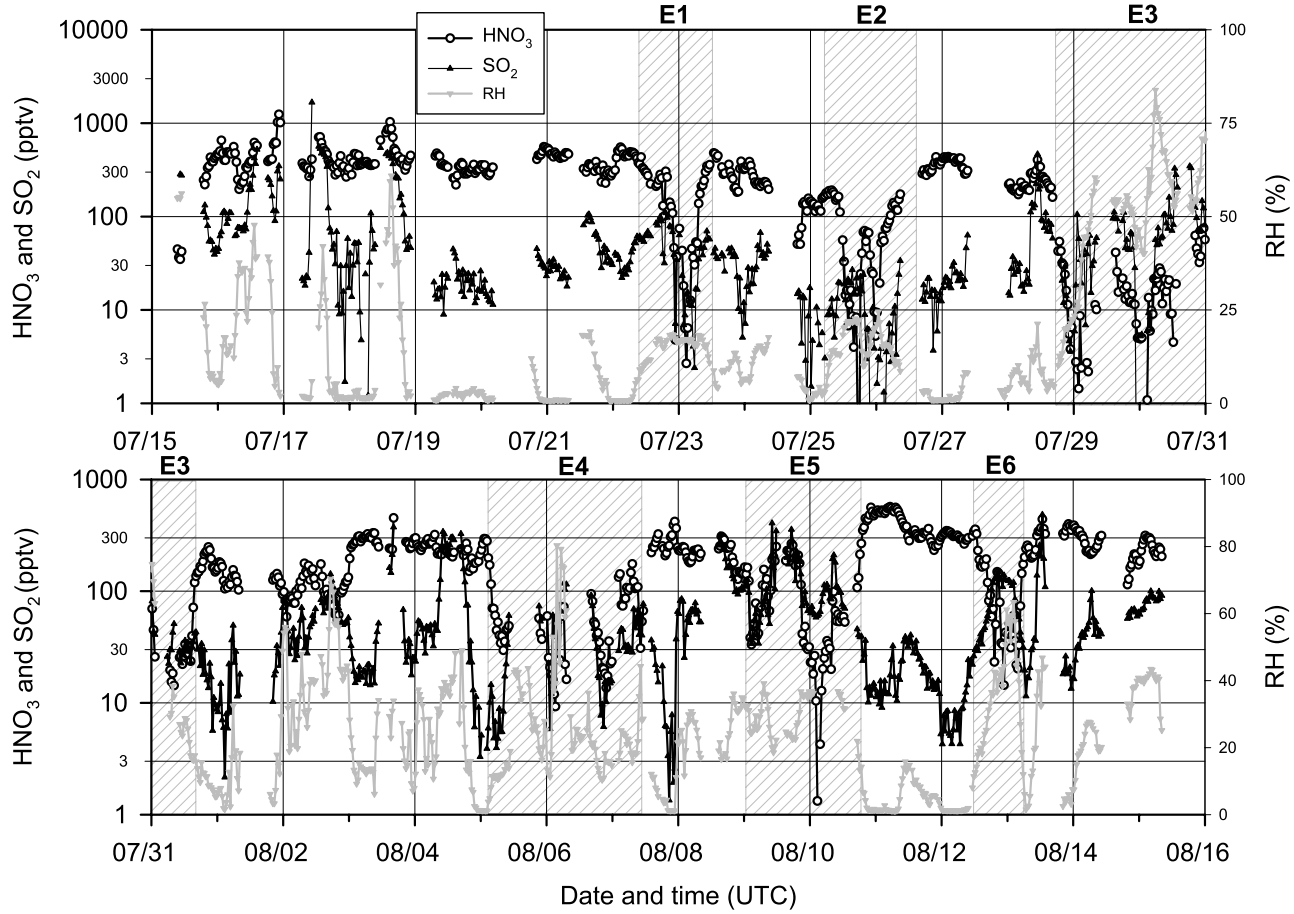

Figure 7. HNO_3, SO_2 and RH time series for MINATROC II. The dust events E1–E6 are denoted hatched in light shading. Note that values below the detection limit are shown as well (compare Table 1 and the associated text). Note further the different scales for the *y* axes.

[29] From these observations we conclude that HNO_3 reacted with mineral dust and that the HNO_3 depletion is only due to the interaction with dust.

2.3.2. SO_2

[30] 30-min average SO_2 VMR for the whole measurement period are shown in Figure 7. Mean VMR for nondust periods amount to 94 and 34 pptv for day and night, respectively. During the dust events the mean SO_2 VMR are even higher. Averaged over all events, day and night VMR are 118 and 47 pptv.

[31] Figure 10 shows SO_2 versus the geometric dust surface. Only for event 1 (E1) a significant anticorrelation is observed and SO_2 decreases with increasing dust down to the detection limit. For E2–E4 and E5, day, no correlation is observed. E5, night, generally shows a negative correlation. However, for high dust surface concentrations (E5, dust surface area >30 $\mu m^2/cm^3$) the correlation becomes positive. Unfortunately, for these increasing SO_2 VMR at high dust concentrations no meteorological data like wind direction etc. exists and an upslope event cannot be excluded. Both for day and night, E6 even shows a significant positive correlation; that is, SO_2 increases with increasing dust.

[32] At first sight, the relatively low RH (Table 4) during the dust events might explain the not observed SO_2 uptake by dust. For RH < 50% *Dentener et al.* [1996] suggest an uptake coefficient γ_{SO_2} of only $3 \cdot 10^{-4}$ (in contrast: RH > 50%: $\gamma_{SO_2} = 0.1$). According to the formalism described in section 3, $\gamma_{SO_2} = 3 \cdot 10^{-4}$ can cause an SO_2 decrease of only <10% for typical parameters (i.e., Fuchs surface $\approx 3\ \mu m^2/cm^3$, reaction time ≈ 3 days), in agreement with the observed data.

[33] On the other hand, for E6 comparatively high RH are observed: $RH_{mean} = 44\%$, see Figure 7 and Table 4. Therefore, according to *Dentener et al.* [1996], an SO_2 uptake by dust was likely. However, an even positive correlation is observed. Moreover, for certain periods of high RH (50–70%) during the dust events SO_2 is in the range of 150 pptv and therefore considerably higher than the mean values with or without dust (e.g., E3: 30.07., 0830–1430 and 2100–0000 UTC or E6: 13.08., 0000–0300 UTC, Figure 7). We conclude that γ_{SO_2} is dominated not only by the prevailing RH but that other parameters must have a great influence on the uptake of SO_2 on mineral dust particles as well. According to *Usher et al.* [2002] who performed investigations by FT-IR spectroscopy and a Knudsen cell reactor, the SO_2 uptake depends strongly on the dust material and the sample mass. Usher presents values for γ_{SO_2} between 0.0007 (China Loess, which consists mainly of silicate) and 0.058 (MgO; in both cases the

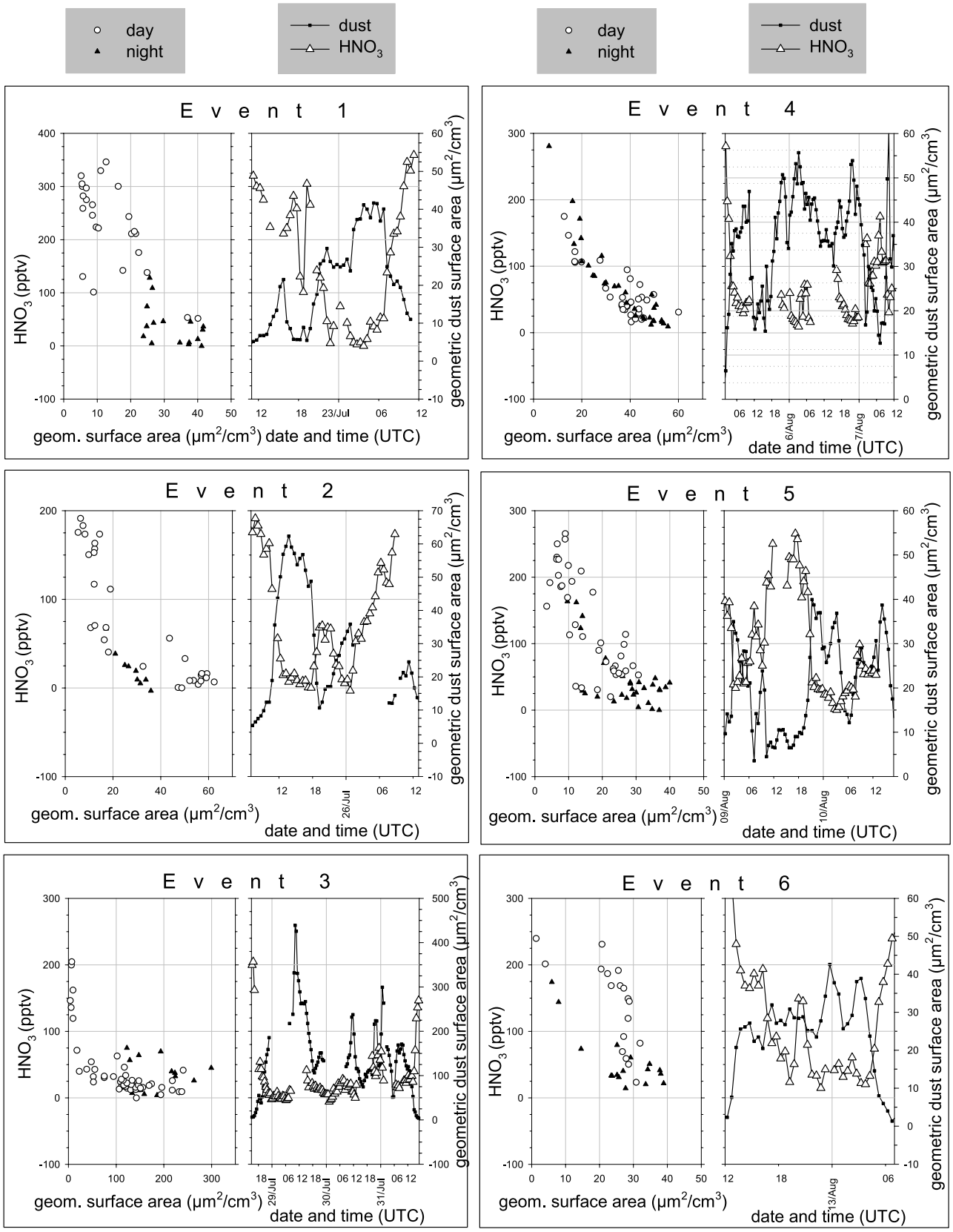

Figure 8. Dust and HNO_3: Correlation plots and time series for the dust events. Note the different scales for the *x* and *y* axes.

Table 3. HNO_3 VMR for Air Masses of African Origin With and Without Dust and of Non-African Origin[a]

	HNO_3, Mean, pptv
Air Masses of African Origin, With Dust	
22 July, 1100 UTC, to 23 July, 1200 UTC	157
25 July, 0700 UTC, to 26 July, 1300 UTC	70
28 July, 1500 UTC, to 31 July, 1700 UTC	27
5 August, 0200 UTC, to 7 August, 1200 UTC	65
9 August, 0000 UTC, to 10 August, 1700 UTC	93
12 August, 1300 UTC, to 13 August, 0700 UTC	99
Air Masses of African Origin, Without Dust	
15 July, 0000 UTC, to 15 July, 0300 UTC	no data
19 July, 1200 UTC, to 20 July, 0000 UTC	424
21 July, 0900 UTC, to 22 July, 1100 UTC	383
23 July, 1200 UTC, to 24 July, 1200 UTC	294
31 July, 1700 UTC, to 1 August, 0300 UTC	177
7 August, 1200 UTC, to 9 August, 0000 UTC	237
10 August, 1700 UTC, to 12 August, 1300 UTC	373
Non-African Air Masses	
15 July, 0300 UTC, to 19 July, 1200 UTC	430
20 July, 0000 UTC, to 21 July, 0900 UTC	430
24 July, 1200 UTC, to 25 July, 0700 UTC	130
26 July, 1300 UTC, to 28 July, 1500 UTC	308
1 August, 0300 UTC, to 5 August, 0200 UTC	192
13 August, 0700 UTC, to 15 August, 0830 UTC	272

[a]The air mass origins base on 5 day backward trajectories of NOAA.

geometric surface was taken into account). Thus the observed behavior at MINATROC II (positive as well as negative correlations) could result both from the RH and from different dust compositions. Unfortunately, information about the dust composition for MINATROC II are not available by now.

3. Determination of the Uptake Coefficient γ_{HNO_3}

[34] For the determination of γ_{HNO_3} we assume that all HNO_3 sources and all sinks other than mineral dust can be neglected. In this case the HNO_3 decrease depends only on the collisional lifetime t_c, the reaction time t_R and γ_{HNO_3} (t_c, t_R: see below). The decrease can then be calculated by a first-order exponential decay model. The curve which fits best to the observed data provides a value for γ_{HNO_3}.

[35] The main source for tropospheric HNO_3 is the reaction of NO_2 with OH. In the region of interest, i.e., NW Africa, modelled NO_2 VMR are of the order of 10–30 pptv [*Dentener and Crutzen*, 1993; *Emmons et al.*, 1997]. Therefore maximal 10–30 pptv HNO_3 can be produced by NO_2 which is negligible compared to the 300 pptv typical for air masses in NW Africa (see end of section 2.3.1). However, nighttime NO_x measurements at MINATROC II performed by the Max Planck Institute for Chemistry, Mainz, Germany, were in the region of 100 pptv [*de Reus et al.*, 2005]. If this NO_x results not only from the island Tenerife itself, an additional HNO_3 production has to be taken into account. Thereby the effective reaction time for the HNO_3 -mineral dust reaction becomes shorter. In this case, the further down calculated uptake coefficient γ_{HNO_3} represents a lower limit.

[36] Since no thunderstorms were observed for the whole measuring period, additional NO_x and therefore HNO_3 from lightnings can be excluded according to reflectivity images of the satellite TOMS (NASA/Goddard Space Flight Center,

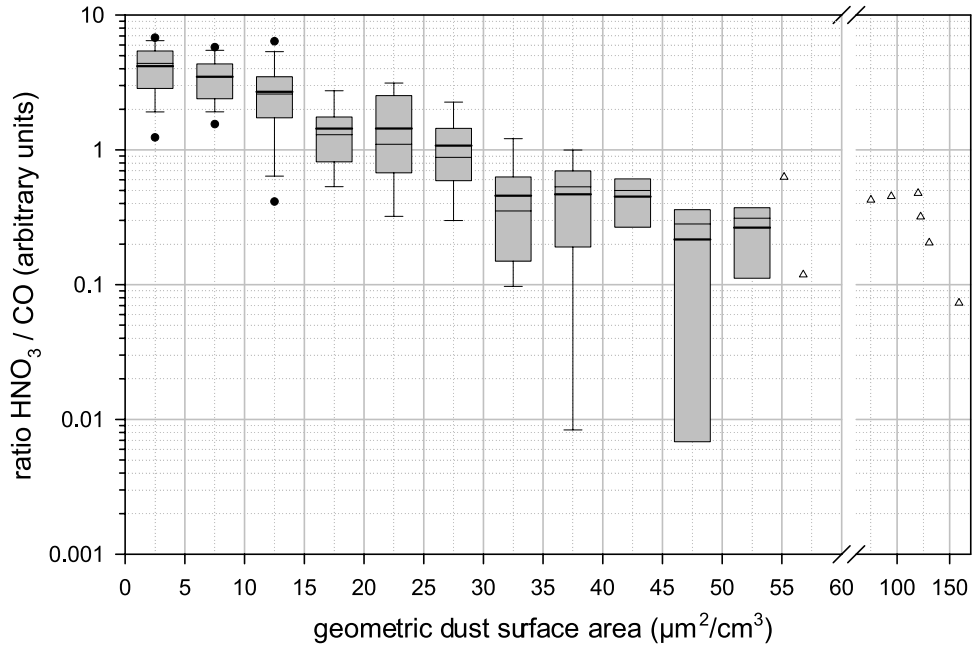

Figure 9. Percentiles of the ratio of HNO_3 to CO as a function of the geometric dust surface area. The latter are binned by 5 $\mu m^2/cm^3$ per bin starting from 0. Circles denote the 5th and 95th, whiskers denote the 10th and 90th and lower and upper lines of the box denote the 25th and 75th percentiles. The thin lines inside the boxes denote the 50th percentile (median), and thick lines denote the mean values. For the calculation of percentiles, at least three data points are required. Therefore single data points are represented by open triangles.

Table 4. Calculated Uptake Coefficients γ_{HNO_3}, Heights of the Air Masses (According to Backward Trajectories of NOAA) and Relative Humidity (RH) for the Six Dust Events[a]

Dust Event	E1	E2	E3	E4	E5	E6	Mean
γ_{HNO_3}	$0.017^{+0.041}_{-0.006}$	$0.05^{+0.040}_{-0.027}$	$0.05^{+0.033}_{-0.024}$	$0.02^{+0.014}_{-0.007}$	$0.03^{+0.017}_{-0.010}$	$0.01^{+0.008}_{-0.007}$	$0.033^{+0.017}_{-0.017}$
Height of air mass during the dust events, m	3200–3800	3300–3700	2200–2700	2500–3000	3100–3200	3300–3800	
RH, %	17	17	13	15	31	44	23

[a]Concerning the RH, only nighttime values are taken into account (except for E3, see text in section 3). For E1, E2, E5 and E6 the RH mean value is presented. For the longer-lasting events E3 and E4 only those values were taken into account at which the HNO_3 VMR did not reach the detection limit since only these values are of interest regarding the calculation of γ_{HNO_3}.

Laboratory for Atmospheres, Greenbelt, MD, USA). The main sinks of HNO_3 are wet and dry deposition as well as the reaction with OH and photolysis. The three last-mentioned are too slow to considerably lower HNO_3 within a few days [*Brasseur et al.*, 1999]. However, wet deposition as a sink can be excluded as well since for the region and time of interest no clouds were observed, see above. Thus the HNO_3 VMR as a function of the reaction time and finally γ_{HNO_3} can be calculated from

$$HNO_3(t_R) = HNO_{3,t_c=\infty} \cdot \exp\left(-\gamma_{HNO_3} \cdot t_R/t_c\right) \quad (1)$$

$$\gamma_{HNO_3} = -\frac{t_c}{t_R} \ln\left(\frac{HNO_3(t_R)}{HNO_{3,t_c=\infty}}\right). \quad (2)$$

[37] $HNO_3(t_R)$ is the VMR at the time t_R measured by the MPI-K with CIMS. $HNO_{3,t_c=\infty}$ is the prevailing VMR just before the dust is introduced into the air mass, i.e., the HNO_3 concentration at the beginning of the reaction (note: $t_c = \infty \iff S_{Fuchs} = 0$). t_c is the collisional lifetime, i.e., the lifetime of HNO_3 molecules with respect to collisions with dust particles. t_c can be obtained as follows: The loss of a species A per unit volume is equal to the rate of collisions of A with a surface S: $-d[A]/dt = \omega$. The kinetic gas theory shows that $\omega = v_{mean} \cdot S \cdot [A]/4$, where v_{mean} is the mean average velocity of species A [*Wayne*, 2000]. After replacing ω, the solution of the differential equation above is $A(t) = A_0\exp(-v_{mean} \cdot S \cdot t/4)$. A comparison with the general solution $A_0\exp(-t/\tau)$ (here: $\tau \equiv t_c$) delivers

$$t_c = 4/(S_{Fuchs} \cdot v_{mean}). \quad (3)$$

[38] S_{Fuchs} is the Fuchs surface (or active surface) of the dust particles per unit volume and can be derived from [*Seinfeld and Pandis*, 1998]. However, the used formula (4) was taken from Matter Engineering AG (Appendix IV of Operating Instructions LQ1-DC, SKM990318-7b) and from (M. Kasper, Matter Engineering AG, personal communication, 2004):

$$S_{Fuchs} = \frac{\pi(A+Q)D^2}{D/2\lambda + [A + Q\exp(-bD/2\lambda)]}. \quad (4)$$

[39] D is the mobility parameter and was measured by means of a DMA (differential mobility analyzer), λ is the mean free path and A, b and Q are the Cunningham fit parameters (A = 1.257; b = 1.10; Q = 0.40). D was measured circa every 2 min and for further investigations averaged over 30 min. Finally, the reaction time t_R in equation (1) is the time that has elapsed since the dust was introduced into the air mass. t_R was obtained from images of the satellite TOMS which showed where the dust intrusion took place. Setting this location into the map of the backward trajectories by NOAA, the reaction time t_R could be estimated. Unfortunately, TOMS did not deliver data for the whole measurement period. In case no data were available (i.e., E4–E6) the simulated optical depth was used to determine the location of the dust intrusion. The latter was calculated using the LMDz-INCA model. A description of the model is given by, e.g., *Bauer et al.* [2004]. Table 5 summarizes the reaction times applied for the six dust events (E1–E6). In general, a mean reaction time was used for every single event. In case t_R differed significantly within one event, different t_R were applied.

[40] Figure 11 shows $HNO_3(t_R)$ measured by CIMS (circles) versus (t_R/t_c) for all dust events. Exceptionally and only for E3 the HNO_3 daytime data are shown since during night no HNO_3 decrease/increase took place. The error bars for HNO_3 result from averaging the data about 30 min and for (t_R/t_c) from the error of t_R, for which we assumed 0.5 days, and from the error of the Fuchs surface which was 20%. The latter results from "D" in equation (4) and therefore from the error propagation of uncertainty of the DMA and the OPC. The negative slope of the function $\ln[HNO_3(t_R)/HNO_{3,t_c=\infty}]$ as a function of t_R/t_c in equation (2) corresponds to γ_{HNO_3}. Thus, from the linear regression lines fitted to the data in Figure 11 (solid lines), a mean value of γ_{HNO_3} for every dust event can be determined. Note that the constant $HNO_{3,t_c=\infty}$ drops out by calculating the slope. Therefore not the above ratio but only $HNO_3(t_R)$ is plotted on the *y* axes. From the dashed lines in Figure 11 the error of γ_{HNO_3} was estimated (principle of minimal and maximal slope, naked eye estimate). The obtained γ_{HNO_3} values for each dust event together with the mean value for all dust events are presented in Table 4 and vary between 0.017 and 0.054. The mean value is 0.033. The regression coefficients shown in Figure 11 are very high ($r \geq 0.82$) except for E1. However, Figure 8 suggests that only a lack of night data causes the relatively weak correlation for E1 in Figure 11.

[41] The values for γ_{HNO_3} shown in Table 4 are somewhat lower compared to those measured in the laboratory by *Fenter et al.* [1995] or *Hanisch and Crowley* [2001] who present values close to 0.1. A reason could be that we underestimate the effective reaction time t_R (see beginning of section 3). On the other hand our values are considerably higher than those measured by *Goodman et al.* [2000] or *Underwood et al.* [2001]. Values of the two last-mentioned

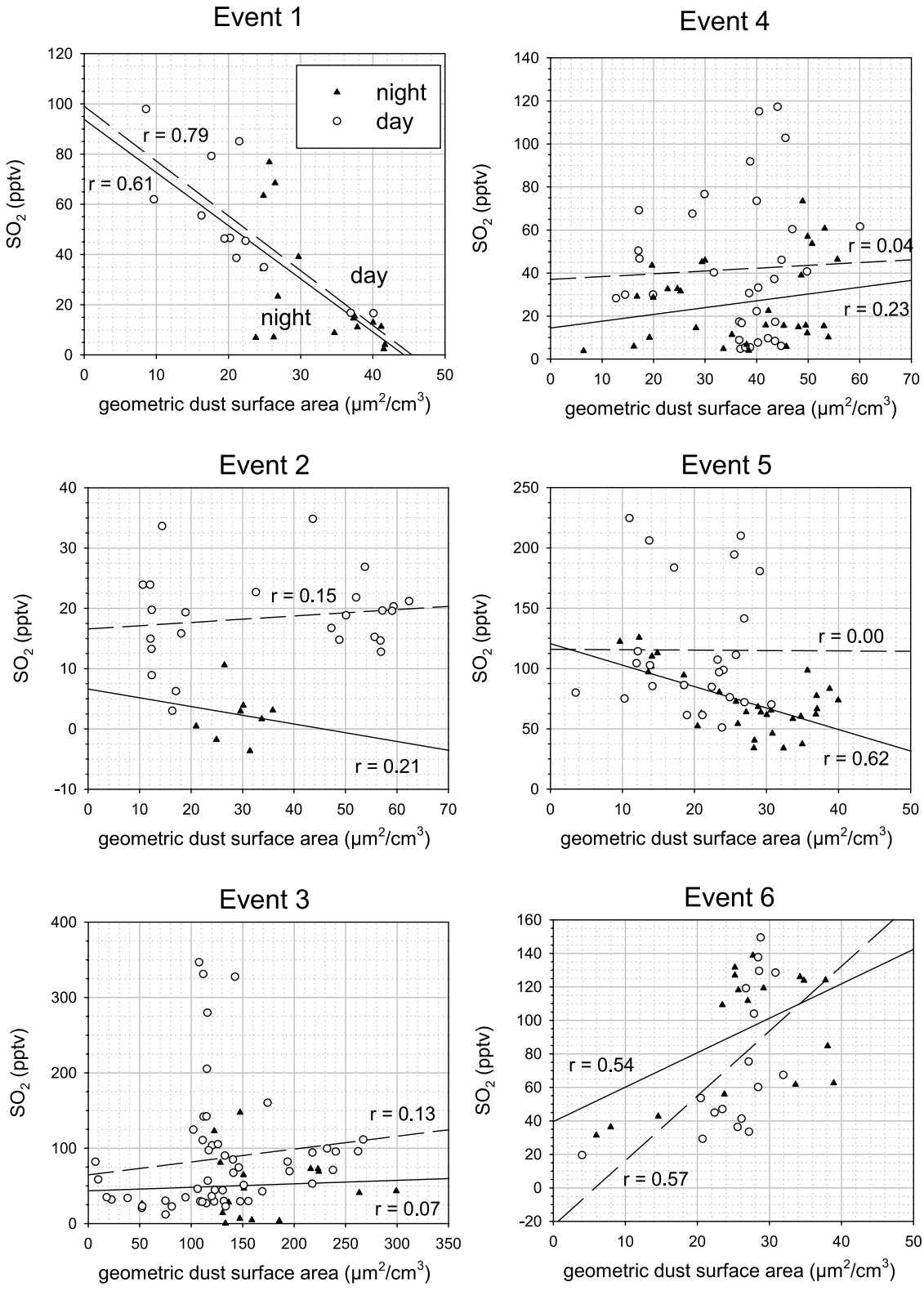

Figure 10. SO_2 versus dust. The lines represent regression curves for night (solid) and day (dashed) values. Solid triangles denote night values, and open circles denote day values. Note the different scales for the *x* and *y* axes.

Table 5. Reaction Times t_R for the Reaction of HNO_3 With Mineral Dust for the Observed Dust Events[a]

	Dust Events							
	E1	E2	E3	E3	E4	E5	E5	E6
Date	22–23 July	25–26 July	28 July	31 July	5–7 August	9 August	10 August	12–13 August
t_R, days	2.5	2.5	1	1.5	2.5	3	4	4

[a]Reaction time t_R is estimated from backward trajectories and satellite images (E1–E3) and from the simulated optical depth (E4–E6), respectively. Only days with decreasing/increasing HNO_3 concentrations are taken into account.

vary between $2.0 \cdot 10^{-5}$ and $6.1 \cdot 10^{-3}$, depending on the RH and the probed material (e.g., $CaCO_3$, CaO, MgO, Saharan sand or China Loess).

[42] For MINATROC II, no significant dependence of γ_{HNO_3} on the RH was observed, in agreement with *Hanisch and Crowley* [2001]. However, the RH was rather low for all dust events (17–44%, mean: 23%, see Table 4). Moreover, a correlation of γ_{HNO_3} with the height of the air masses could not be observed, suggesting a low influence of the temperature on the interaction of mineral dust with HNO_3. In Table 4 we present the minimal and maximal heights for each dust event as described in section 2.3.1. For example, for E2 and E3, the heights varied between 2200 m and 3700 m and the RH were similar, whereas γ_{HNO_3} stayed almost constant at 0.053. On the other hand, for E1 and E6 the heights were similar but the RH varied between 17 and 44%. Again, a constant value for γ_{HNO_3} was measured ($\gamma_{HNO_3} = 0.017$).

4. Atmospheric Implications: Influence on O_3

[43] Via photolysis and the reaction with OH, HNO_3 represents a source for NO_x and thus for tropospheric ozone [*Dentener and Crutzen*, 1993; *Jacob et al.*, 1996]. An HNO_3 decrease due to the reaction with mineral dust should therefore result in a decrease of O_3. For example, in the presence of dust, *de Reus et al.* [2000] observed an O_3 decrease of 30–40% during the ACE 2 experiment and conclude that ~50% of the O_3 decrease is due to a depletion of HNO_3.

[44] The results from MINATROC II partly confirm these observations. Ozone mixing ratios were measured by the Izaña Observatory and kindly put at our disposal. The ozone time series is shown in Figure 12. During the dust events the O_3 VMR are significantly lower than outside the events and the O_3 mean value drops from ~60 ppbv (without dust) down to ~40 ppbv (with dust). This corresponds to an O_3 decrease of 33%, in agreement with the above mentioned result of *de Reus et al.* [2000]. This behavior can be seen more clearly from Figure 13, where the O_3 percentiles are plotted as a function of the dust surface area. The latter are binned by 5 $\mu m^2/cm^3$ per bin. At first the O_3 VMR decreases with increasing dust surface area. At dust concentrations of about 25–30 $\mu m^2/cm^3$ it stays almost constant at ~35 ppbv. For almost the same dust surface (30 $\mu m^2/cm^3$) HNO_3 was removed completely from the atmosphere, i.e., without HNO_3 no further O_3 depletion was observed. This suggests that the ozone decrease in the presence of dust is dominated by the HNO_3 depletion and that no or only little O_3 uptake on dust occurred. Following the approach described in section 3 (equation (1)), one obtains the same result: Typical reaction times (0.5–5 days), collisional lifetimes (E3: 200 s; other events: 2000 s) and uptake coefficients ($\gamma_{O_3} = 3 \cdot 10^{-6} \ldots 3 \cdot 10^{-5}$ [*Dentener et al.*, 1996; *de Reus et al.*, 2000; *Bauer et al.*, 2004]) lead to an uptake of O_3 on mineral dust of 0.0 to 6.3% which is much to small to explain the observed decrease of about 33%.

[45] We mention here that just as for HNO_3 African but dust-free air masses (see Table 3) did not show an atypical behavior regarding the O_3 concentrations. On the basis of 5 day backward trajectories (NOAA), mean ozone VMR for those air masses varied between 51 and 72 ppbv with an overall mean value of 60 ppbv ± 11 ppbv. Moreover, air masses of non-African origin contained between 49 and 67 ppbv with an overall mean value of 59 ppbv ± 13 ppbv which is in the same region as the values mentioned above.

[46] Finally we point out that the decrease of O_3 in the presence of dust could possibly result from altered photochemical forces as well. However, recent publications conclude that the effects of photochemical forces through aerosols on the tropospheric O_3 cycle are negligible [*Fiore et al.*, 2002; *Liao et al.*, 2003] or that these effects are even positively correlated with O_3 (remote northern hemisphere, July), i.e., in the presence of dust O_3 increases because of photochemistry [*Bian and Zender*, 2003]. However, the latter as well state that this is a second-order effect.

5. Summary and Outlook

[47] During the MINATROC II campaign, six periods of medium and high atmospheric dust load were observed. According to backward trajectories, these air masses originated from the Sahara or the Sahel. For every dust event the HNO_3 mixing ratio decreased with increasing dust concentrations and for geometric dust surfaces higher than 30 $\mu m^2/cm^3$ the HNO_3 detection limit was reached. Tracers for polluted air masses like CO showed no atypical behavior during the dust events, indicating that these air masses were not just free of pollutants like HNO_3. Further on, African air masses in nondust periods contained just as much HNO_3 as other dust-free air masses. From these observations we conclude that an HNO_3-mineral dust reaction took place.

[48] Assuming that all HNO_3 sinks other than mineral dust and all HNO_3 sources can be neglected, we calculated uptake coefficients γ_{HNO_3} for six dust events of Saharan and Sahelian origin. γ_{HNO_3} varied between 0.017 and 0.054 with a mean value of 0.033 ± 0.017. However, it might be that we underestimate the effective reaction time for the mineral dust-HNO_3 reaction because of an additional HNO_3 source in the reaction zone. Referring to this, our values for γ_{HNO_3} represent a lower limit. These values compare more or less well with those determined in the laboratory by *Fenter et al.* [1995] or *Hanisch and Crowley* [2001] who suggest $\gamma_{HNO_3} = 0.1$. A dependence of γ_{HNO_3} on the RH was not

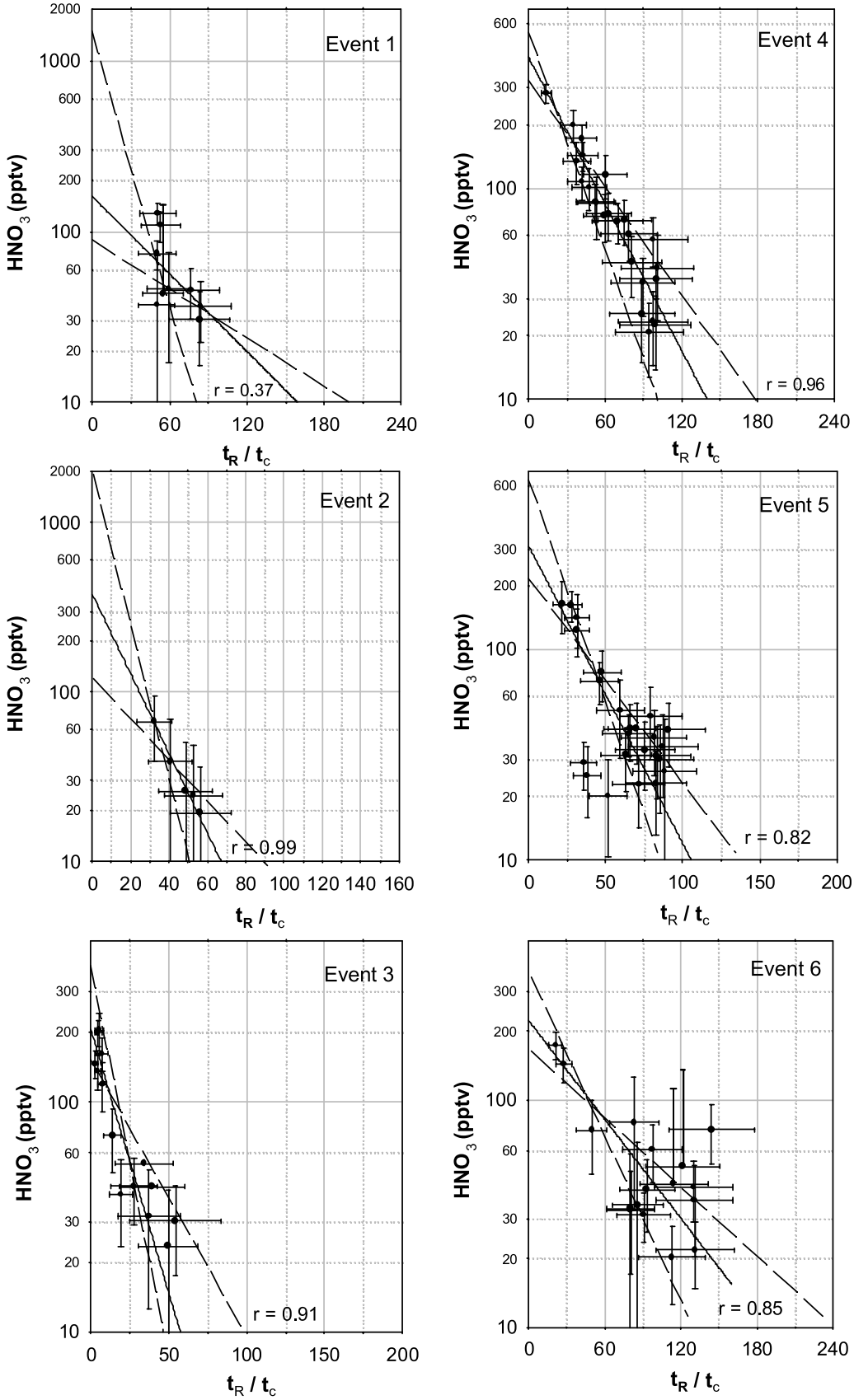

Figure 11. Calculation of γ_{HNO_3} from the regression line fitted to the HNO_3 decay as a function of the ratio t_R/t_c. Only night data are taken into account. For details, see text.

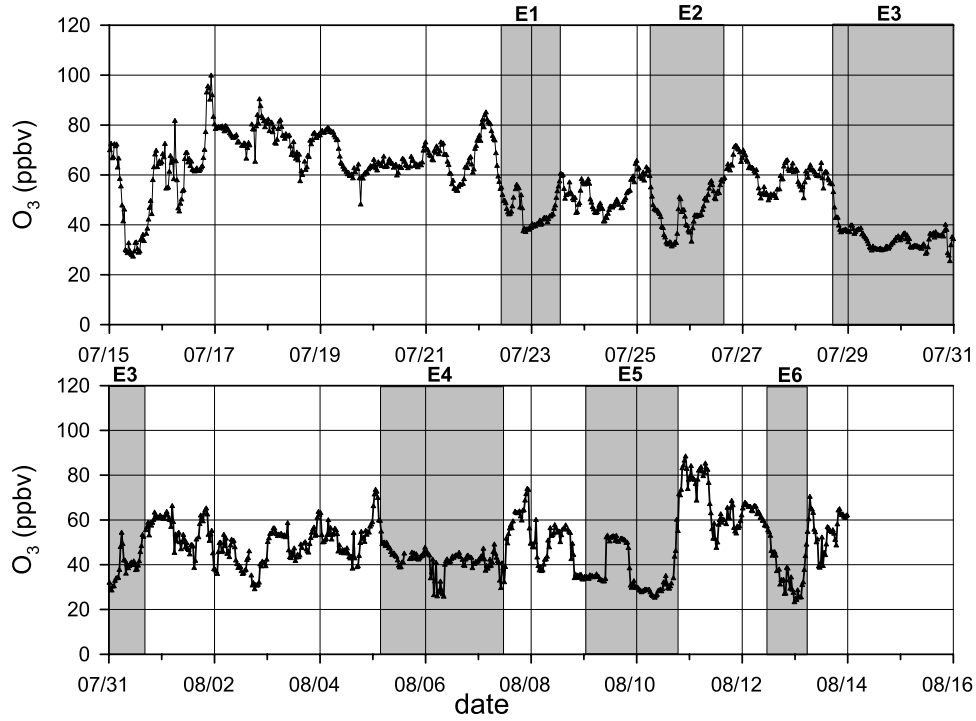

Figure 12. Ozone VMR for the whole measurement period. The dust events E1–E6 are highlighted in light shading.

observed. However, during the dust events the RH rarely reached above 40%.

[49] Besides the HNO_3 depletion a decrease of O_3 of the order of 30% was observed during the events. Our data suggest that this decrease is not due to an adsorption of ozone on dust but it results only from the removal of HNO_3.

[50] In contrast, a significant SO_2-mineral dust anticorrelation was not observed. In some cases the correlation was positive, in some negative and in most of the cases no correlation was detected. Moreover we conclude that not only the RH but other parameters (possibly the dust composition) must have a great influence on γ_{SO_2}.

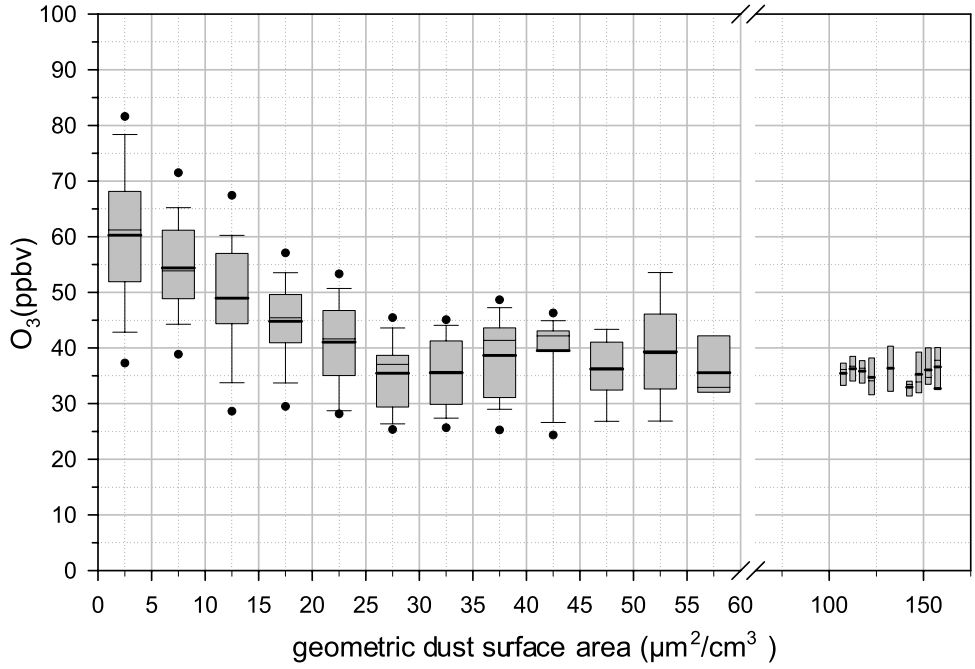

Figure 13. Percentiles of the measured ozone mixing ratios versus geometric dust surface area for the whole measurement period. For details, see caption of Figure 9.

[51] **Acknowledgments.** This study is part of the EU-funded project MINATROC (EVK2-CT-1999-00003) under the 5th Framework Program. We like to thank the MINATROC community and the technical staff of the MPI-K.

References

Andreae, M. O., R. J. Charlson, F. Bruynseels, H. Storms, R. van Grieken, and W. Maenhaut (1986), Internal mixture of sea salt, silicates and excess sulfate in marine aerosols, *Science*, *232*, 1620–1623.

Arnold, F. (1980), Multi-ion complexes in the stratosphere—Implications for trace gases and aerosol, *Nature*, *284*, 610–611.

Balkanski, Y., et al. (2003), The Mt. Cimone, Italy, free tropospheric campaign: Principal characteristics of the gaseous and aerosol composition from European pollution, Mediterranean influences and during African dust events, *Atmos. Chem. Phys. Disc.*, *3*, 1753–1776.

Bauer, S. E., Y. Balkanski, M. Schulz, D. A. Hauglustaine, and F. Dentener (2004), Global modelling of heterogeneous chemistry on mineral aerosol surfaces: Influence on tropospheric ozone chemistry and comparison to observations, *J. Geophys. Res.*, *109*, D02304, doi:10.1029/2003JD003868.

Bian, H., and C. S. Zender (2003), Mineral dust and global tropospheric chemistry: Relative roles of photolysis and heterogeneous uptake, *J. Geophys. Res.*, *108*(D21), 4672, doi:10.1029/2002JD003143.

Brasseur, G. P., J. J. Orlando, and G. S. Tyndall (1999), *Atmospheric Chemistry and Global Change*, Oxford Univ. Press, New York.

Dentener, F. J., and P. J. Crutzen (1993), Reaction of N_2O_5 on tropospheric aerosols: Impact on the global distributions of NO_x, O_3 and OH, *J. Geophys. Res.*, *98*, 7149–7163.

Dentener, F. J., G. R. Carmichael, Y. Zhang, J. Lelieveld, and P. J. Crutzen (1996), Role of mineral aerosol as a reactive surface in the global troposphere, *J. Geophys. Res.*, *101*, 22,869–22,889.

de Reus, M., F. Dentener, A. Thomas, S. Borrmann, J. Ström, and J. Lelieveld (2000), Airborne observations of dust aerosol over the North Atlantic Ocean during ACE 2: Indications for heterogeneous ozone destruction, *J. Geophys. Res.*, *105*(D12), 15,263–15,275.

de Reus, M., H. Fischer, R. Sander, V. Gros, R. Kormann, G. Salisbury, R. Van Dingenen, J. Williams, M. Zöllner, and J. Lelieveld (2005), Observations and model calculations of trace gas scavenging in a dense Saharan dust plume during MINATROC, *Atmos. Chem. Phys.*, *5*, 1787–1803.

Emmons, L. K., et al. (1997), Climatologies of NO_x and NO_y: A comparison of data and models, *Atmos. Environ.*, *31*, 1851–1904.

Fenter, F. F., F. Caloz, and M. J. Rossi (1995), Experimental evidence for the efficient "dry deposition" of nitric acid on calcite, *Atmos. Environ.*, *29*, 3365–3372.

Finlayson-Pitts, B. J., and J. N. Pitts Jr. (2000), *Chemistry of the Upper and Lower Atmosphere*, Elsevier, New York.

Fiore, A. M., D. J. Jacob, I. Bey, R. M. Yantosca, B. D. Field, A. C. Fusco, and J. G. Wilkinson (2002), Background ozone over the United States in summer: Origin, trend, and contribution to pollution episodes, *J. Geophys. Res.*, *107*(D15), 4275, doi:10.1029/2001JD000982.

Goodman, A. L., G. M. Underwood, and V. H. Grassian (2000), A laboratory study of the heterogeneous reaction of nitric acid on calcium carbonate particles, *J. Geophys. Res.*, *105*, 29,053–29,064.

Guimbaud, C., F. Arens, L. Gutzwiller, H. W. Gäggeler, and M. Ammann (2002), Uptake of HNO_3 to deliquescent sea-salt particles: A study using the short-lived radioactive isotope tracer ^{13}N, *Atmos. Chem. Phys.*, *2*, 249–257.

Hanisch, F., and J. N. Crowley (2001), Heterogeneous reactivity of gaseous nitric acid on Al_2O_3, $CaCO_3$ and atmospheric dust samples: A Knudsen cell study, *J. Phys. Chem.*, *105*, 3096–3106.

Hanke, M., B. Umann, J. Uecker, F. Arnold, and H. Bunz (2003), Atmospheric measurements of gas-phase HNO_3 and SO_2 using chemical ionization mass spectrometry during the MINATROC field campaign 2000 on Monte Cimone, *Atmos. Chem. Phys.*, *3*, 417–436.

Jacob, D., et al. (1996), Origin of ozone and NO_x in the tropical troposphere: A photochemical analysis of aircraft observations over the South Atlantic basin, *J. Geophys. Res.*, *101*, 24,235–24,250.

Knop, G., and F. Arnold (1985), Nitric acid vapour measurements in the troposphere and lower stratosphere by chemical ionisation mass spectrometry, *Planet. Space Sci.*, *33/II*, 983–986.

Korhonen, P., M. Kulmala, A. Laaksonen, Y. Viisanen, R. McGraw, and J. Seinfeld (1999), Ternary nucleation of H_2SO_4, NH_3 and H_2O in the atmosphere, *J. Geophys. Res.*, *104*, 26,349–26,353.

Liao, H., P. J. Adams, S. H. Chung, J. H. Seinfeld, L. J. Mickley, and D. J. Jacob (2003), Interactions between tropospheric chemistry and aerosols in a unified general circulation model, *J. Geophys. Res.*, *108*(D1), 4001, doi:10.1029/2001JD001260.

Neumann, J. A., L. G. Huey, T. B. Ryerson, and D. W. Fahey (1999), Study of inlet materials for sampling atmospheric nitric acid, *Environ. Sci. Technol.*, *33*(7), 1133–1136.

Penner, J. E., et al. (2001), Aerosols, their direct and indirect effects, in *Climate Change 2001: The Scientific Basis—Contribution of Working Group I to Chemical and Physical Characteristics*, edited by J. T. Houghton et al., pp. 291–336, Cambridge Univ. Press, New York.

Seinfeld, J., and S. N. Pandis (1998), *Atmospheric Chemistry and Physics*, John Wiley, Hoboken, N. J.

Uecker, J., M. Hanke, and F. Arnold (2001), First speciated atmospheric measurements of HO_2 and organic peroxy radicals (ΣRO_2) by chemical conversion/ion molecule reaction mass spectrometry (ROXMAS) before, during and after the major mineral dust intrusion on Monte Cimone during the first MINATROC field campaign in June–July 2000, paper presented at 8th European Symposium on the Physico-Chemical Behaviour of Atmospheric Pollutants, Torino, Italy, 17–20 Sept.

Ullerstam, M., R. Vogt, S. Langer, and E. Ljungström (2002), The kinetics and mechanism of SO_2 oxidation by O_3 on mineral dust, *Phys. Chem. Chem. Phys.*, *4*, 4694–4699.

Underwood, G. M., C. H. Song, M. Phadnis, G. R. Carmichael, and V. H. Grassian (2001), Heterogeneous reactions of NO_2 and HNO_3 on oxides and mineral dust: A combined laboratory and modelling study, *J. Geophys. Res.*, *106*, 18,055–18,066.

Usher, C. R., H. Al-Hosney, S. Carlos-Cuellar, and V. H. Grassian (2002), A laboratory study of the heterogeneous uptake and oxidation of sulfur dioxide on mineral dust particles, *J. Geophys. Res.*, *107*(D23), 4713, doi:10.1029/2002JD002051.

Wayne, R. P. (2000), *Chemistry of Atmospheres*, Oxford Univ. Press, New York.

Wilhelm, S., S. Eichkorn, D. Wiedner, L. Pirjola, and F. Arnold (2004), Ion-induced aerosol formation: New insights from laboratory measurements of mixed cluster ions $HSO_4^-(H_2SO_4)_a(H_2O)_w$ and $H^+(H_2SO_4)_a(H_2O)_w$, *Atmos. Environ.*, *38*, 1735–1744.

Yu, F., and R. P. Turco (2000), Ultrafine aerosol formation via ion-mediated nucleation, *Geophys. Res. Lett.*, *27*, 883–886.

H. Aufmhoff, F. Arnold, M. Hanke, C. Schaal, J. Uecker, and B. Umann, Atmospheric Physics Division, Max-Planck-Institut für Kernphysik, Heidelberg D-69117, Germany. (bernd-umann@web.de)

Y. Balkanski, Laboratoire des Sciences du Climat et de l'Environnement, Centre National de la Recherche Scientifique/Commissariat à l'Energie Atomique, F-91191 Gif-sur-Yvette, France.

R. Van Dingenen, Institute for Environment and Sustainability, Joint Research Centre, European Commission, I-21020 Ispra, Italy.

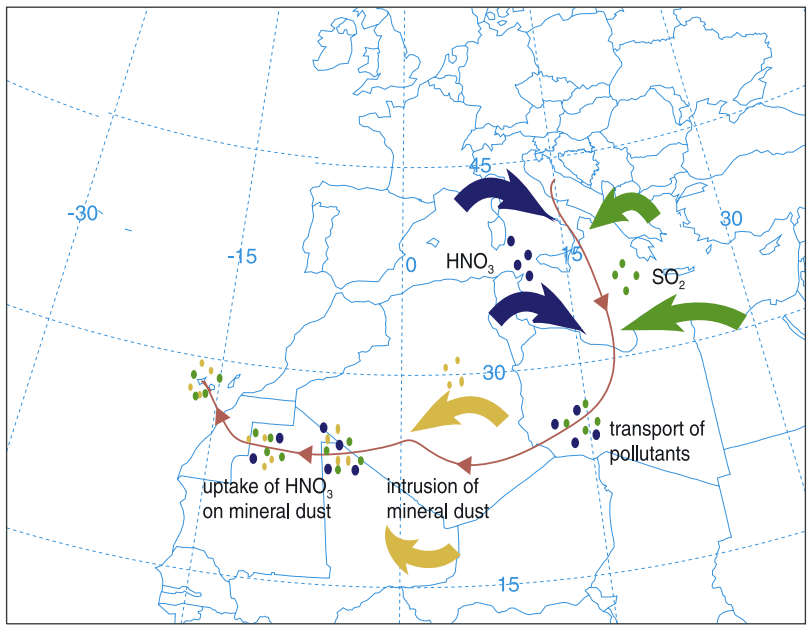

Figure 1. "Atmospheric flow reactor:" Pollutants such as HNO_3 (blue spots) or SO_2 (green spots) are injected into the atmosphere over south Europe or North Africa. Over northwest Africa these air masses mix with uplifted mineral dust (yellow spots), and heterogeneous reactions may take place. Here, only HNO_3 reacted with mineral dust. The picture is based on the backward trajectory from 29 July 2002, 1200 UTC, a day with high atmospheric dust load (NOAA, Washington, D. C., United States).

Figure 2. Panorama of the measuring site Izaña. The picture was taken from the roof of our measuring container.

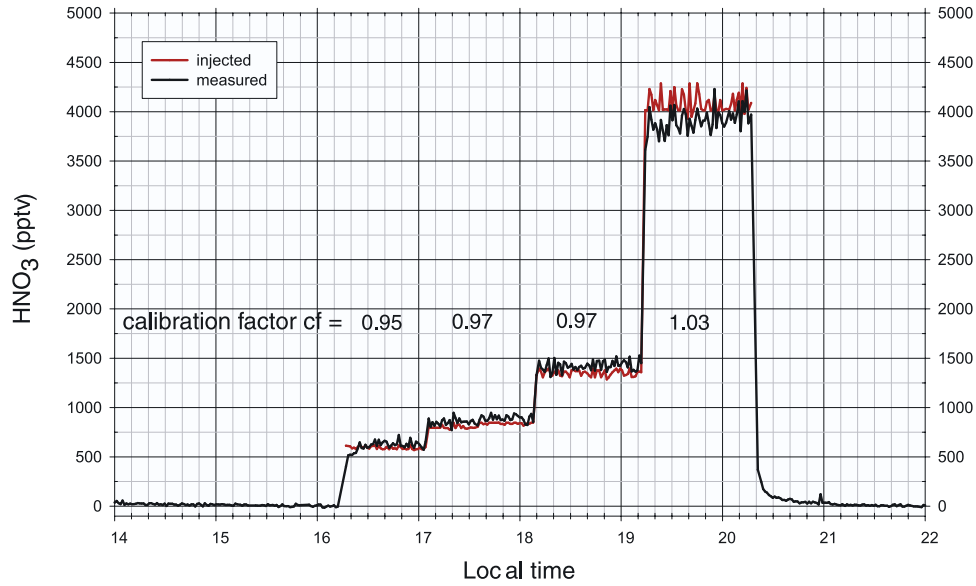

Figure 4. Test for the linearity of the HNO_3 calibration factor cf = $HNO_{3,\ injected}/HNO_{3,\ measured}$. Linearity is given.